Understanding Mineralogical and Geochemical Evolution in Geothermal Reservoirs through Reactive Transport Modelling

Dale Emet Altar[1], Sadiq J. Zarrouk[1] and Eylem Kaya[1]

[1] Department of Engineering Science, University of Auckland, Private Bag 92019, Auckland, New Zealand

dalt507@aucklanduni.ac.nz

Keywords: *Reactive transport simulation, Fluid-rock interaction, Natural state reservoir model, TOUGHREACT™*

ABSTRACT

Reactive transport modelling plays a crucial role in unravelling the dynamics of geothermal reservoirs as they evolve over time. By utilising these models, we gain a deeper understanding of the temporal progression of mineral alteration and its influence on the reservoir's characteristics. This information empowers us to effectively manage and safeguard these valuable resources while offering critical insights into sustainable development.

This study was designed to understand the mineralogical and geochemical evolutionary process of conventional geothermal reservoirs. An idealised 3D large-scale numerical model was set up to comply with the prevailing conditions in a two-phase-liquid-dominated geothermal reservoir. The models were established to assess the long-term fluid and rock interaction in geothermal systems and gain insights into the hydrothermally altered rocks.

The results of our reactive transport modelling study provide information about the deep geochemical processes that occur during fluid circulation within the reservoir. The model captures the natural processes that alter the chemical composition of minerals in the reservoir over time, highlighting spatial mineral alteration patterns, their impact on porosity and permeability, and how these factors influence flow paths. Additionally, the study investigates the mineralogical and geochemical changes induced by the influx of CO_2, H_2S and H_2. The model also explores the effects of fluid chemistry and geologic structures on underground fluid circulation.

1. INTRODUCTION

The evolution of geothermal reservoirs is a complex interplay of geological, tectonic, and hydrothermal processes occurring over vast geological time scales. Understanding this evolution is crucial for sustainable management and utilisation of geothermal resources.

In this paper, we present a generalised overview of the geochemical and flow parameters that manifest during the development of a two-phase liquid-dominated system. The models offer insight into the factors controlling the dynamic transformations during their formation stages via interactions of water, minerals and heat during their geochemical alteration journey.

The significance of the evolutionary history from a geothermal perspective is primarily due to its implications for the origins of major geological features, thermodynamics, and understanding of the geochemical processes that shape these reservoirs. These attributes play an important role in understanding the underlying structural influences in contemporary settings, alteration sequences, the potential mechanisms driving various processes, and the prospective minerals that might form along the pathways of deep fluid circulation and the dynamic changes in fluid chemistry within the reservoir.

A natural state model was created for an idealised, theoretical geothermal reservoir incorporating reactive transport. The initial unreacted formation hosting the geothermal reservoir was taken to be tholeiitic basalt, using the mineralogical data from Passarella (2021) with additional analysis from Altar et al. (2022, 2023). The initial fluid and the recharge were assumed to be groundwater, while the upflowing fluid had similar chemistry with the addition of dissolved CO_2, H_2S, and H_2. The study aims to establish approximate natural state conditions, which can be utilised to assess various operational/development opportunities for geothermal reservoirs.

The reservoir parameters, various aspects of model design, and kinetic and thermodynamic parameters must be investigated in detail to obtain accurate and realistic predictions for the evaluation of geothermal systems by modelling. It should be recognised that running reactive transport models on this scale presents a significant challenge. Overcoming this challenge involves conducting numerous iterations of simulations, which are computationally demanding and time-intensive, even with the use of many simplifying assumptions. The complexities of the geochemical and physical processes occurring within geothermal reservoirs can lead to simulation convergence issues. The TOUGHREACT simulations were carried out in part on the NeSI Pan Cluster at the University of Auckland to reduce the computational cost associated with these model challenges.

2. REACTIVE TRANSPORT MODEL

The model was set up using the numerical simulation tool TOUGHREACT4™ (Sonnenthal et al., 2021). TOUGHREACT™ is a comprehensive non-isothermal multi-component reactive fluid flow and geochemical transport simulator developed by introducing reactive chemistry into the framework of TOUGH2™ (Pruess, 1991; Pruess et al., 1999). The fluid equation of state EOS1 was selected, which provides fluid properties for pure water, typical for hydrothermal problems. EOS1 was deemed appropriate as the highest modelled temperature in this study was only 374°C. SUPCRTBL (Zimmer et al., 2016) was used to estimate the necessary thermodynamic data for all chemical species and reactions in the model. PyTOUGH (Croucher, 2011, 2015; Wellmann et al., 2012, 2014) was used to automate creating and editing model grids and data files, visualising chemical results, and automation of model runs. TIM (Yeh et al., 2013) was likewise used for model visualisation.

2.1 Fluid Transport Parameters

The grid block structure used for this study is shown in Figure 1. The 3D rectangular grid covers a total area of 34 km × 28

ISSN 2703-4275

km with a depth of 6 km. Side boundary blocks were set up along the perimeter of the modelled volume, with areas of 2 km × 2 km, while the inner blocks have areas of 1 km × 1 km. Each column was divided into 15 layers below ground level, with 12 additional layers above ground to represent volcanic terrain. All model blocks are single porosity.

Figure 1: W-E Slice view of the model grid structure indicating the rock types.

Eight rock types were used in the model to capture the heterogeneity of the geothermal system and represent key features: an atmospheric boundary (dfalt), ground surface (grd01), an intermediate lithology between the ground and the cap rock (grd02), the cap rock (cap01), the host reservoir lithology (res01), an upper basement lithology (dep02), a deeper basement lithology (dep01), and finally one to represent the perimeter boundary blocks (bnd01) (Figure 1). Grain density (2600 kg/m^3), porosity (10%), heat conductivity (1.5 W/m•K), and rock grain specific heat (900 J/kg•K) are the same for all rock types. The primary distinguishing factor among these rock types was their permeability, which is crucial in simulating fluid flow within the reservoir. The permeabilities of each rock type and their depth locations are summarised in Table 1.

Table 1: Model rock types, their permeabilities, and depth location

Rock type	K_x, mD	K_y, mD	K_z, mD	Depth, m
dfalt	1000	1000	1000	
grd01	100	100	100	0 – 100
grd02	0.1	0.1	0.1	100 – 300
cap01	0.1	0.1	0.01	300 – 600
res01	50	50	5	600 – 3000
dep01	0.01	0.01	0.1	3000 – 4000
dep02	0.01	0.01	0.1	4000 – 6000
bnd01	10	10	10	

Heat generators were added to all blocks in the bottom layer of the grid. The heat rates per block were calculated from the block face area along the x-y plane and heat flux values. A baseline heat flux of 0.06 W/m^2 (Jaupart et al., 2007; Davies and Davies, 2010) was used except for an area with a radius of 4 km taken to overlay the heat source for the geothermal system. This area was assigned a heat flux of 0.15 W/m^2, comparable to values reported by Hardee and Larson (1980) and Studt and Thompson (1969) for geothermal areas. A mass input of 100 kg/s with an enthalpy of 1300 kJ/kg was defined to represent an upflow, assigned to a single block. A top view of the bottommost layer showing the heat inputs and mass input block is given in Figure 2.

Before any reactive transport runs, the flow model was run from initial conditions set at 25°C and 1 bar for 1.5×10^{13} s with just the baseline heat flux across all bottom layer blocks and the constant atmospheric boundary in place (25°C and 1 bar). That provided the new initial conditions used for the reactive transport simulations: the initial pressure and temperature gradients before the addition of the localised higher heat flux and the upflow.

The side boundary blocks were then assigned volumes of ≥10^{50} m^3 to maintain their temperatures and pressures at the initial conditions. Likewise, that ensures that they maintain their chemical concentrations throughout the model runs. It was done to simulate open boundaries.

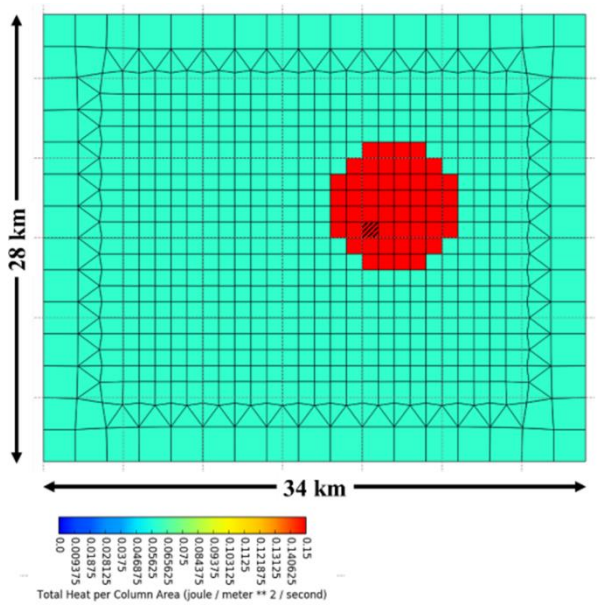

Figure 2: Bottom layer of the model grid structure. Colours represent the heat fluxes (W/m^2). The red circular area represents the underlying heat source with higher heat flux. Hatched red block indicates the position of the mass upflow.

2.2 Geochemical Parameters

2.2.1 Initial Mineral Assemblage and Fluid Chemistry

Reactive calculations were limited to the intermediate lithology between the ground and the cap rock (grd02), the cap rock (cap01), the host reservoir lithology (res01), and the upper basement lithology (dep02); remaining rock types were considered to be inert. The reactive blocks were taken to be unreacted basalt whose mineral assemblage and volume fractions were adapted from data by Passarella (2021) supplemented with the additional analysis based on the models of Altar et al. (2022, 2023). Secondary minerals observed in the experimental work of Passarella (2021) were included in the system, along with other representative minerals observed in hydrothermal environments. The primary minerals in the basalt and their initial volume fractions are listed in Table 2, along with the secondary minerals considered in the model. Secondary minerals were assigned initial volume fractions of 0.0%.

The initial fluids in all model blocks were assumed to be groundwater, with a chemical profile adapted from Morgenstern et al. (2005) and supplemented with data from Popugaeva et al. (2018) for aluminium. This includes the atmospheric boundary and side boundary blocks.

The upflow was assumed to have the same chemical composition as the groundwater with the addition of

dissolved CO_2, H_2S and H_2. Conceptually, dissolved gases come from the underlying geothermal heat source (e.g., magmatic intrusion). Partial pressures for the gases were adapted from Coudrain-Ribstein et al. (1998) and Arnórsson (1985). That the fluid maintains most chemical properties of the groundwater is a simplifying assumption for the model and can be revisited in future work. The chemical profiles for the initial and upflow fluids are given in Table 3.

Table 2: Starting mineralogy and volume fractions in the model for the reactive blocks, as well as modelled secondary minerals.

	Mineral	% Vol
Primary	Anorthite	45.3%
	Albite	14.2%
	Sanidine	0.22%
	Augite	28.0%
	Olivine	1.9%
	Titanomagnetite	3.6%
	Glass	6.8%
Secondary	Sphene, Calcite, Magnesite, Siderite, Dolomite, Wollastonite, Chlorite, Grossular, Magnetite, Quartz, Chalcedony, Am Silica, Illite, Montmorillonite, Anhydrite, Kaolinite, Celadonite, Pyrite, Epidote, Stilbite, Laumontite, Wairakite	

Table 3: Assumed composition for the initial and upflow fluids in the model. Concentration values are in molal units, while partial pressures are in bar.

Component	Initial Fluid	Upflow Fluid
Temperature, °C	21	300
Pressure, bar	1	200
pH_T	7	4.87
Na^+	3.64E-04	3.64E-04
K^+	3.73E-05	3.73E-05
Ca^{2+}	1.59E-04	1.59E-04
Mg^{2+}	9.34E-05	9.34E-05
Fe^{2+}	3.58E-07	3.58E-07
Al^{3+}	3.26E-05	3.26E-05
Cl^-	2.06E-04	2.06E-04
SO_4^{2-}	4.02E-05	4.02E-05
$H_4SiO_{4,aq}$	3.83E-04	3.83E-04
$Ti(OH)_{4,aq}$	1.00E-10	1.00E-10
H_2S_{aq}	3.00E-07	5.57E-03
$H_{2,aq}$	1.00E-07	3.52E-03
$CO_{2,aq}$	1.00E-08	2.99E-02
P_{H2S}		0.15
P_{H2}		0.8
P_{CO2}		2.0

2.2.2 Mineral Reaction Parameters

Mineral reactions were primarily modelled to be kinetically controlled, except for titanite (sphene), calcite, magnesite, siderite, and dolomite, which were assumed to be under local equilibrium. The general transition state theory rate law (Eqn 1) is used to model reaction kinetics in TOUGHREACT™.

$$r_n = \pm k_n A_n \prod_{i=1}^{N} {a_i}^{m_i} \left[1 - \left(\frac{Q}{K_n}\right)^{\theta}\right]^{\eta} \quad (1)$$

Here, r_n is the reaction rate of the nth mineral in the system (mol kg^{-1} s^{-1}); k_n is the rate constant (mol m^{-2} s^{-1}); A_n is the reactive surface area (m^2 kg^{-1}); $\Pi a_i m_i$ represents the activities of species to which rates are dependent; Q is the activity product for the reaction; K_n is the equilibrium constant for the reaction; and the exponents η and θ describe the relationship of the rate to chemical affinity.

Parameters used to calculate the dissolution rate constants (k_n) as a function of temperature were adopted from Palandri & Kharaka (2004). The parameters for basalt glass were adopted from Gislason and Oelkers (2003) and Oelkers and Gislason (2001). The dissolution rate parameters were also used to represent precipitation kinetics for the same minerals. The reader is referred to the studies mentioned above for the rate constant parameter values.

Guidance on estimating the reactive surface area (RSA) for fractured media is available in Appendix G of the TOUGHREACT user manual (Sonnenthal et al., 2021). The initial value calculated for the RSA was 157 m^2/m^3. Typically, this is reduced by two to three orders of magnitude for use with the model to account for the general observation that field reaction rates are orders slower than laboratory rates (Aradóttir et al., 2012; Gislason and Eugster, 1987; White and Brantley, 2003). For this model, however, the value was reduced by five orders of magnitude. This is because the higher reaction rates modelled at higher surface area values resulted in calculation instabilities and errors. The reduction was deemed acceptable as the study is more concerned with long-term alteration effects.

SUPCRTBL (Zimmer et al., 2016) was used to calculate the equilibrium constants for the dissociation of aqueous complexes and the dissolution of minerals at temperatures between 0 °C and 350 °C. At temperatures below 100°C, the equilibrium constants were evaluated at 1 bar and above that at the corresponding saturation pressures of water. The redox control was assumed to be by the $H^+/H_{2,aq}$ redox couple.

Equilibrium constants for mineral solid solutions were estimated, assuming they were ideal. The stoichiometric saturation model proposed by Thorstenson and Plummer (1977) was selected to calculate the equilibrium constants.

Another element of the reactive transport model is the relationship between porosity and permeability. As minerals dissolve and precipitate, the porosity of the system changes; subsequently, permeability will also change, and this may have a significant effect on the fluid flow across the modelled reservoir. A porosity-permeability function following the Verma-Pruess relation (Eqn 2) was defined. This function is based on the premise that flow channels in permeable media are subject to pore throat effects (Verma and Pruess, 1988). When porosity decreases, narrow sections of the fluid flow paths may close, resulting in a loss of permeability without a complete loss of porosity.

$$\frac{k}{k_i} = \left[\frac{\phi - \phi_c}{\phi_i - \phi_c}\right]^n \quad (2)$$

Here, k is the permeability at time t, k_i is the initial rock permeability, ϕ is the porosity at time t, ϕ_i is the initial rock porosity, ϕ_c is the critical porosity, the porosity at which permeability is zero, and n is an exponent. For this model, the

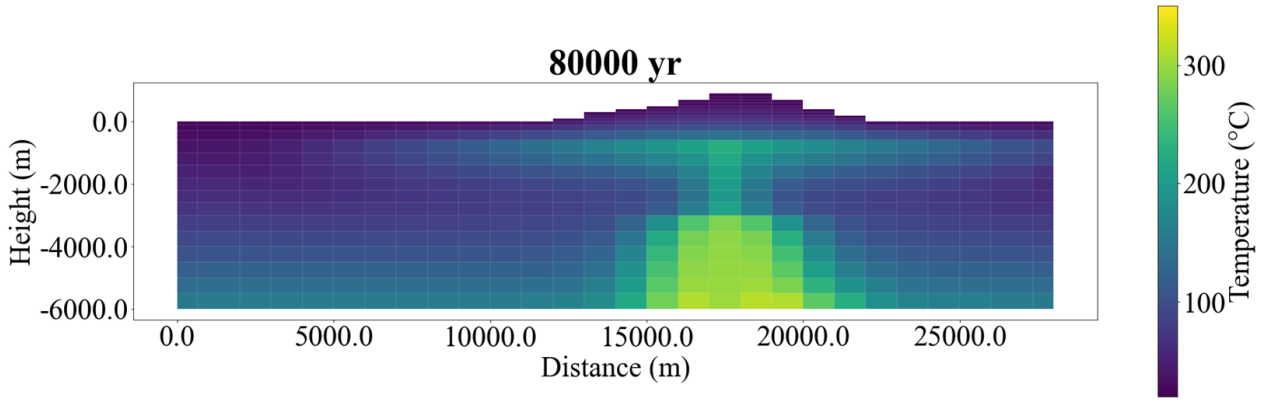

Figure 3: Temperature profile at 80000 years

critical porosity was set to 7.5% and the exponent to a value of 2.

2. RESULTS

At the end of 80000 years, the modelled system had achieved a relatively stable temperature profile (Figure 3). However, it is not yet the fully developed profile expected from a natural state model that only accounts for fluid flow and energy balances. Despite this, significant mineral alterations are expected to have occurred within this time frame based on the model results.

Of the primary minerals, significant dissolution of glass (Figure 4) and olivine occurred. Towards the end of the modelled 80000-year period, augite began to dissolve in the blocks depleted of glass and olivine. Neither titanomagnetite nor plagioclase dissolved in the model.

Mica, quartz, chalcedony, secondary albite, zeolite, chlorite and epidote formed from the resulting dissolution products. Small amounts of calcite and siderite were also deposited (<1%) in the presence of dissolved carbon dioxide. Magnetite and pyrite were likewise observed in small quantities. Volume fractions of select secondary minerals at the end of the modelled time are shown in Figure 5.

The mineral dissolution and precipitation processes resulted in a decrease in porosity along the path of the upflow. This is attributed to the larger molar volumes of the secondary minerals compared to the primary minerals. The reduction in porosity resulted in permeability reduction, as shown in Figure 6 for the modelled permeability along the z-direction. Despite the porosity reduction, the modelled change in permeability is insufficient to cause a significant difference in flow path behaviour.

The evolution of fluid chemistry was also tracked. To contextualise the modelled values, they were reviewed against measured fluid chemistry data from the Krafla geothermal field (Gudmundsson and Arnórsson, 2002). Krafla stands as the closest field analogue to the idealised model at the time of writing this paper due to similarities in the host rock and the fluid chemistry of the recharge.

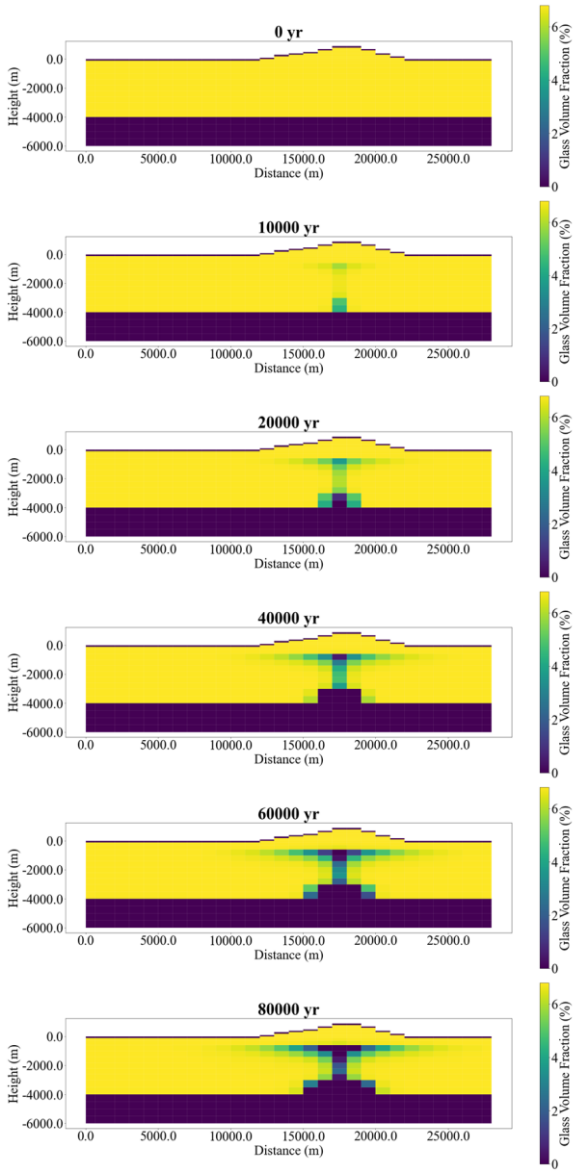

Figure 4: Dissolution profile of glass over time

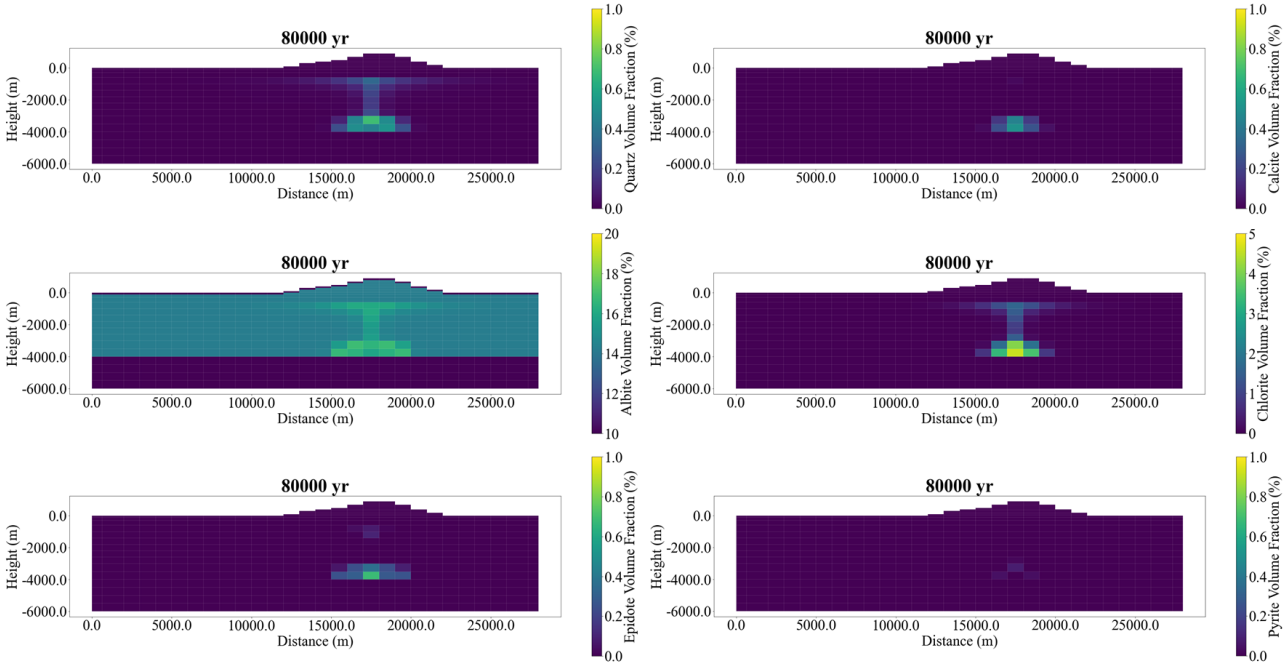

Figure 5: Volume fractions of quartz, calcite, albite, chlorite, epidote and pyrite in the modelled reservoir after 80000 years

A summary of modelled concentrations and data from Gudmundsson and Arnórsson (2002) for selected chemical species are provided in Table 4. For example, chloride concentrations increased over time in the modelled reservoir from the progressive dissolution of glass, being the only source of chloride in the model. At the end of 80000 years, chloride concentrations across the model ranged between 0.3 to 0.85 mmol/kg, comparable to Krafla's data, though this is expected to evolve further at longer time scales (Figure 7). Modelled concentration values for sulfate are lower than the measured data.

In general, modelled concentrations of chemical species in the fluids are higher than values from the available field data, which can be seen for the sodium, potassium, silica and aluminium data in Table 4. For this model, this is attributed mainly to the high dissolution rate of glass compared to the precipitation rates of the secondary minerals in the model (two to four orders of magnitude less), a result of the kinetic parameters used.

Table 4: Modelled fluid chemistry data and available production fluid chemistry data for the Krafla geothermal field from Gudmundsson and Arnórsson (2002). Values in parentheses are the averages of the available data.

Species	Model, mmol/kg	Krafla, mmol/kg
Na^+	8.7 – 26	1.0 – 8.3 (4.6)
K^+	2.6 – 7.7	0.13 – 0.57 (0.35)
Ca^{2+}	~0	0.003 – 0.095 (0.04)
Cl^-	0.3 – 0.85	0.2 – 1.2 (0.6)
SO_4^{2-}	0.02 – 0.04	0.02 – 3.1 (1.2)
H_4SiO_4	1.0 – 18.7	2.1 – 7.3 (5.0)
Al^{3+}	0.04 – 0.37	0.007 – 0.04 (0.02)

Silica concentrations are particularly high in colder regions of the modelled reservoir. The dissolution of the primary minerals mobilised significant amounts of silica. In the upflow region where temperatures are higher, quartz and chalcedony precipitation rates are higher, resulting in concentrations closer to quartz saturation. However, at lower temperature regions, the precipitation rates are orders of magnitude slower, such that the modelled silica concentrations remain high. Given that similar concentrations are not observed in natural geothermal systems, the rate balance between silica mobilisation and precipitation requires further review.

3. CONCLUSION

The results obtained from reservoir-scale models can provide valuable insights into the evolution of geothermal reservoirs over geologic time. This includes information on the locations of mineral deposits, alteration effects on reservoir permeabilities, and the evolution of reservoir fluid chemistry. It can also provide useful information throughout the productive life of the resource. Calibrated reservoir-scale reactive transport models may likewise give additional insights into sectors of existing geothermal reservoirs where there are limited data and surveys.

Based on the results, a steady state has not yet been achieved after modelling 80000 years. Therefore, the reservoir fluid chemistry and mineral alterations are expected to evolve further with time. The same applies to the porosity and permeability across the modelled reservoir. Future work for this study will involve extending the modelled time duration to observe further changes. Reviews and conduct of sensitivity tests on the reaction modelling and flow parameters are also being done to evaluate the robustness of the model assumptions.

One key challenge that remains is the uncertainty of mineral reaction kinetic and equilibrium parameters, especially at high temperatures. The same can be said about related parameters like the reactive surface area, all of which affect

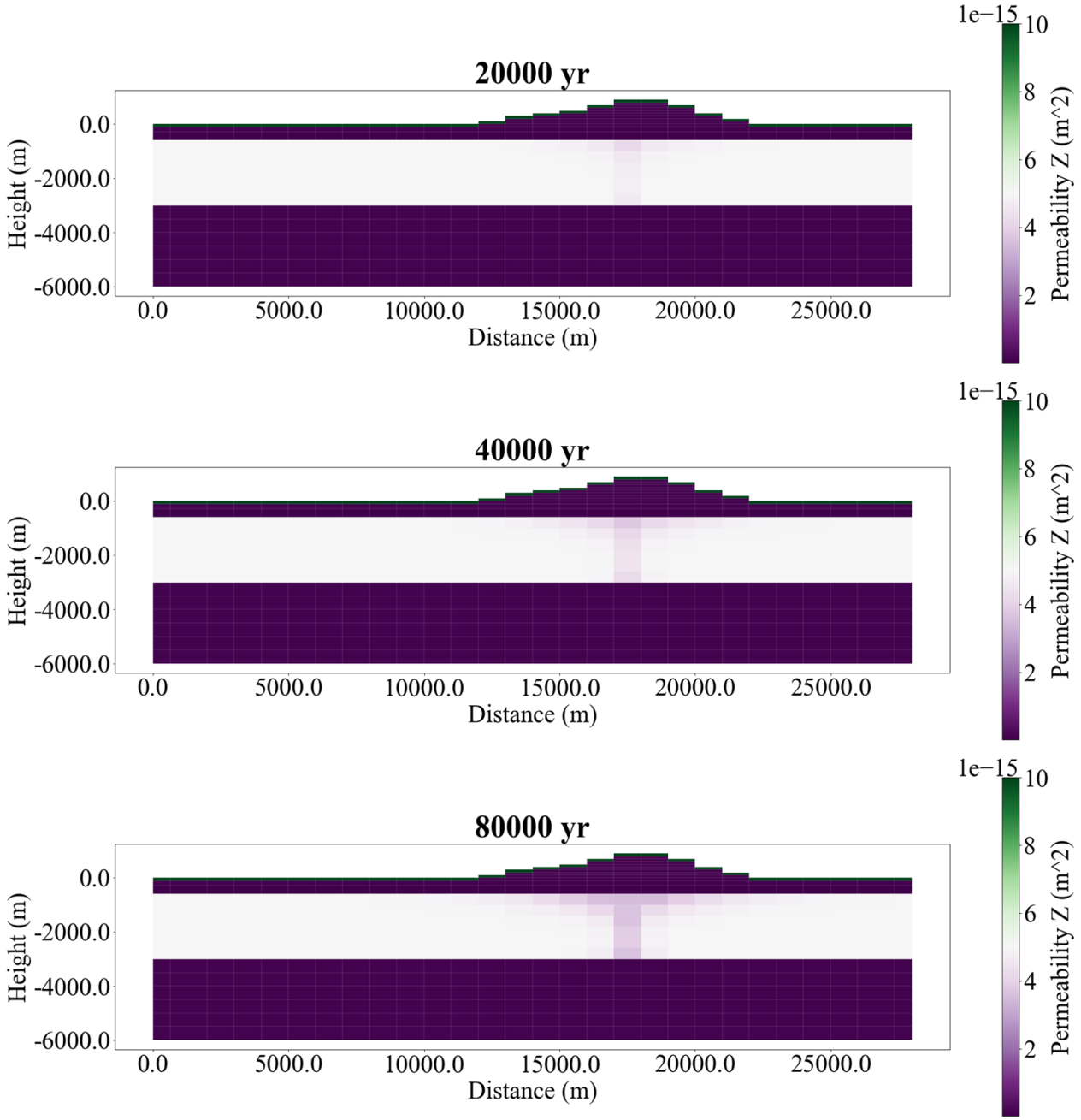

Figure 6: Modelled permeability change over time

the modelled geochemical alterations. Despite the uncertainties, there was sufficient partial agreement between the model and the properties of typical hydrothermal environments. Further refinement of assumptions can improve overall model behaviour.

Reactive transport models of this scale require significant computing resources, even with simplifying assumptions. One key observation is that calculation speeds significantly decreased with an increasing number of model elements. A finer grid structure that works for a fluid transport model may not be optimal for a reactive transport model.

Additionally, a model limitation is that it does not capture the full complexity of the sequence of events throughout the development of the reservoir, e.g., it was assumed that the heat source and upflow appeared at a single point in time and that there was no mineral alteration before this. The modelling framework and conceptual model will significantly impact the usefulness of results from these types of models.

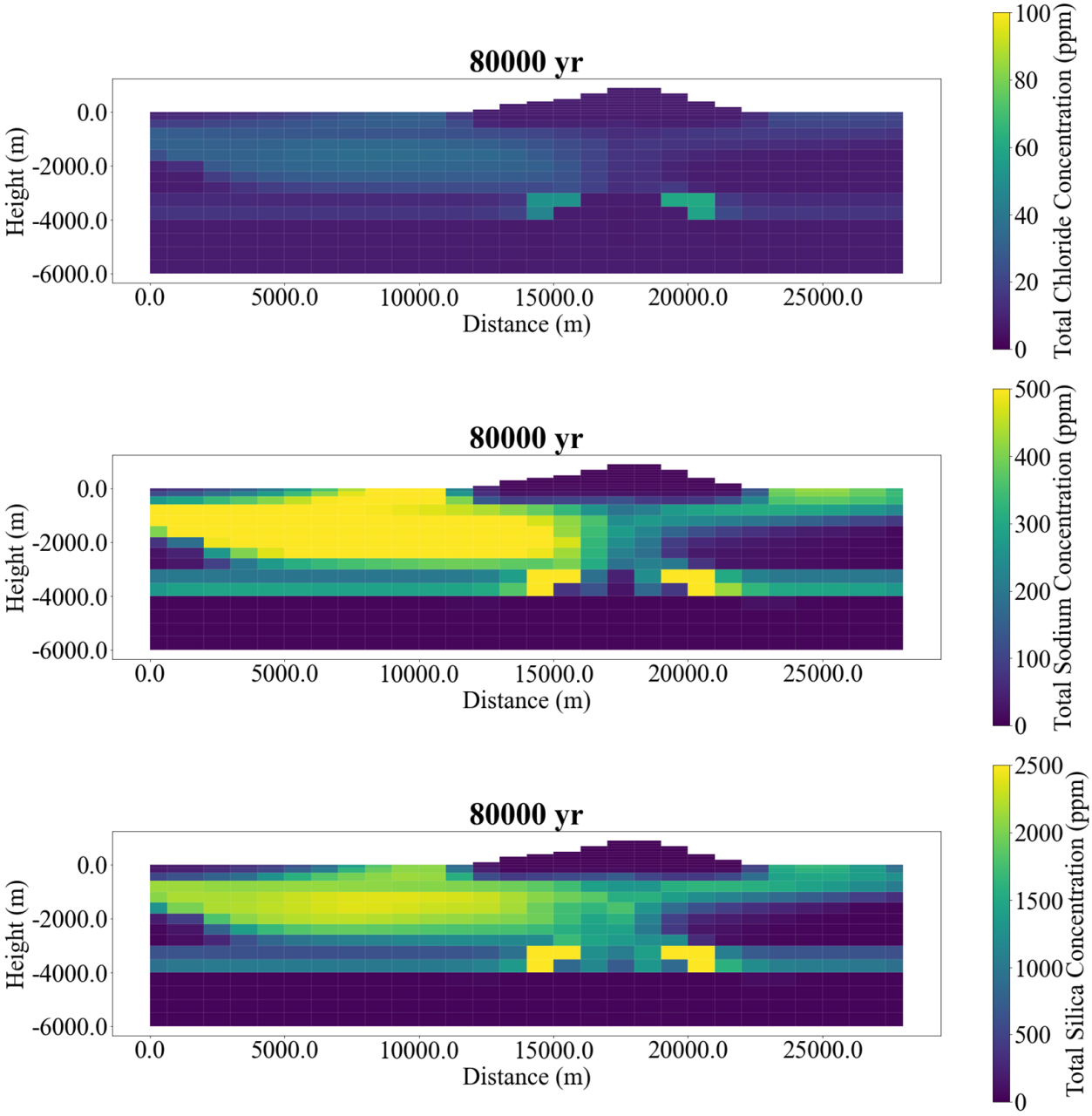

Figure 7: Modelled Cl, Na and $H_4SiO_{4,aq}$ concentrations across the reservoir after 80000 years

ACKNOWLEDGEMENTS

This work was supported by the University of Auckland Doctoral Scholarship. We also thank the NZ Ministry of Business, Innovation and Employment for funding the work through MBIE Research Programmes: GNS-MBIE00150 "Geothermal: Next Generation" and "Reversing Carbon Emissions in the Geothermal Energy Industry: Template for Emission-Intensive Industries" projects.

We also wish to acknowledge the use of New Zealand eScience Infrastructure (NeSI) high-performance computing facilities as part of this research. New Zealand's national facilities are provided by NeSI and funded jointly by NeSI's collaborator institutions and through the Ministry of Business, Innovation & Employment's Research Infrastructure programme. URL https://www.nesi.org.nz.

REFERENCES

Altar, D.E., Kaya, E., Zarrouk, S.J., Passarella, M., Mountain, B.W., 2022. Numerical geochemical modelling of basalt-water interaction under subcritical conditions. *Geothermics 105*, 102520.

Altar, D.E., Kaya, E., Zarrouk, S.J., Passarella, M., Mountain, B.W., 2023. Reactive transport modelling under supercritical conditions. *Geothermics 111*, 102725.

Aradóttir, E.S.P., Sonnenthal, E.L., Björnsson, G., Jónsson, H., 2012. Multidimensional reactive transport modeling of CO2 mineral sequestration in basalts at the Hellisheidi geothermal field, Iceland. *International Journal of Greenhouse Gas Control 9*, 24-40.

Arnórsson, S., 1985. Gas pressures in geothermal systems. *Chemical Geology 49*, 319-328.

Bakht, M.S., 1997. Borehole geology and hydrothermal alteration of well KJ-28, Krafla high-temperature area, NE-Iceland.

Coudrain-Ribstein, A., Gouze, P., de Marsily, G., 1998. Temperature-carbon dioxide partial pressure trends in confined aquifers. *Chemical Geology 145*, 73-89.

Croucher, A.E., 2011. PyTOUGH: a Python scripting library for automating TOUGH2 simulations.

Croucher, A., 2015. Recent developments in the PyTOUGH scripting library for TOUGH2 simulations.

Davies, J.H., Davies, D.R., 2010. Earth's surface heat flux. *Solid earth 1*, 5-24.

Gislason, S.R., Eugster, H.P., 1987. Meteoric water-basalt interactions. II: A field study in N.E. Iceland. *Geochimica et Cosmochimica Acta 51*, 2841-2855.

Gislason, S.R., Oelkers, E.H., 2003. Mechanism, rates, and consequences of basaltic glass dissolution: II. An experimental study of the dissolution rates of basaltic glass as a function of pH and temperature. *Geochimica et Cosmochimica Acta 67*, 3817-3832.

Gudmundsson, B.T., Arnórsson, S., 2002. Geochemical monitoring of the Krafla and Námafjall geothermal areas, N-Iceland. *Geothermics 31* (2), 195-243.

Jaupart, C., Labrosse, S., Lucazeau, F., Mareschal, J.C., 2007. 7.06-temperatures, heat and energy in the mantle of the earth. *Treatise on geophysics 7*, 223-270.

Morgenstern, U., Reevers, R.R., Daugney, C.J., Cameron, S., Gordon, D., 2005. Groundwater age and chemistry, and future nutrient loads for selected Rotorua lakes catchments.

Oelkers, E.H., Gislason, S.R., 2001. The mechanism, rates and consequences of basaltic glass dissolution: I. An experimental study of the dissolution rates of basaltic glass as a function of aqueous Al, Si and oxalic acid concentration at 25°C and pH = 3 and 11. *Geochimica et Cosmochimica Acta 65*, 3671-3681.

Palandri, J.L., Kharaka, Y.K., 2004. A Compilation of Rate Parameters of Water-Mineral Interaction Kinetics for Application to Geochemical Modeling. U.S. Geological Survey.

Passarella, M., 2021. Basalt - fluid interactions at subcritical and supercritical conditions: An experimental study.

Popugaeva, D., Kreyman, K., Ray, A.K., 2018. Study of aluminium in groundwater using chemometric methods. *Environmental technology 41*, 1691-1699.

Pruess, K., Oldenburg, C.M., Moridis, G.J., 1999. TOUGH2 User's Guide Version 2.

Pruess, K., 1991. TOUGH2-A general-purpose numerical simulator for multiphase fluid and heat flow.

Sonnenthal, E., Spycher, N., Xu, T., Zheng, L., 2021. TOUGHREACT V4. 12-OMP and TReactMech V1. 0 Geochemical and Reactive-Transport User Guide.

Studt, F.E., Thompson, G., 1969. Geothermal heat flow in the North Island of New Zealand. *New Zealand Journal of Geology and Geophysics 12*, 673-683.

Thór Gudmundsson, B., Arnórsson, S., 2002. Geochemical monitoring of the Krafla and Námafjall geothermal areas, N-Iceland. *Geothermics 31*, 195-243.

Thorstenson, D.C., Plummer, L.N., 1977. Equilibrium criteria for two-component solids reacting with fixed composition in an aqueous phase; example, the magnesian calcites. *American Journal of Science 277*, 1203-1223.

Verma, A., Pruess, K., 1988. Thermohydrological conditions and silica redistribution near high-level nuclear wastes emplaced in saturated geological formations. *Journal of Geophysical Research: Solid Earth 93*, 1159-1173.

Wellmann, J.F., Croucher, A., Regenauer-Lieb, K., 2012. Python scripting libraries for subsurface fluid and heat flow simulations with TOUGH2 and SHEMAT. *Computers & Geosciences 43*, 197-206.

Wellmann, J.F., Finsterle, S., Croucher, A., 2014. Integrating structural geological data into the inverse modelling framework of iTOUGH2. *Computers & Geosciences 65*, 95-109.

White, A.F., Brantley, S.L., 2003. The effect of time on the weathering of silicate minerals: why do weathering rates differ in the laboratory and field?. *Chemical Geology 202*, 479-506.

Yeh, A., Croucher, A.E., O'Sullivan, M.J., 2013. TIM-Yet another graphical tool for TOUGH2.

Zimmer, K., Zhang, Y., Lu, P., Chen, Y., Zhang, G., Dalkilic, M., Zhu, C., 2016. SUPCRTBL: A revised and extended thermodynamic dataset and software package of SUPCRT92. *Computers & Geosciences 90*, 97-111.